Electronic Supplementary Material (ESI) for Nanoscale.

Supporting Information for

One- and Two-Photon Brightness of Proteins Interacting with Gold. A Closer Look at Gold-Insulin Conjugates

Dipankar Bain, Hao Yuan, Anna Pniakowska, Agata Hajda, Charlène Bouanchaud, Fabien Chirot, Clothilde Comby-Zerbino, Virginie Gueguen-Chaignon, Vlasta Bonačić-Koutecký, Joanna Olesiak-Banskà, Željka Sanader Maršić and Rodolphe Antoine

Experimental

Materials. Tetrachloroauric acid trihydrate ($HAuCl_4 \cdot 3H_2O$), sodium hydroxide (NaOH), 1,3-Diphenylisobenzofuran (DPBF), and 2,5-Dihydroxybenzoic acid (DHB) were purchased from Sigma-Aldrich. Recombinant human insulin was purchased from Life Technologies Corporation. New methylene blue (NMB) was purchased from TCI. Milli-Q water with a resistivity of 18.2 MΩ cm was used for all experiments.

Synthesis and purification of insulin-gold conjugate. Insulin-gold conjugates was synthesized using an earlier reported protocol with modification.[1] Typically, 100 mg insulin was dissolved in 5 mL ultrapure water and stirred for 5 minutes in room temperature. Next, 5 mM of 5mL Au3+ solution was added to white color suspension and the color turns to yellowish white. The reaction mixture was continued for another 5 minutes. Then, 400 µL of 1 M NaOH solution was added to adjust the pH around 11.5, and the solution color changed to yellow and finally light yellow within 5 minutes. Tuning pH is an efficient strategy to modulate the interactions between amino-acids and metals.[2] The reaction mixture was placed at 37°C for 4 hours. The synthesis protocol is given in Figure S1. To remove excess metal salts (Au+ and Na+), as-synthesized Insulin-Au NCs was purified by using centrifugation with 3kDa molecular weight cut off (MWCO) centrifuge tube (Figure S2). The centrifugation was carried out at 12,000 RPM at 18º C. 4 mL of Insulin-Au samples were taken in centrifuge tube and allowed for centrifugation for 30 minutes. After that supernatant portion was kept and 2 mL water was added. Then this solution was further used for centrifugation for another 30 minutes and the process was continued for total 7-times. Finally, the precipitate of conjugates was collected and stored at 4º C for further use. The synthesis process involves of using commercially available biomolecule insulin as a stabilizing agent, The synthesis process does not involve any harsh reaction conditions, particularly avoiding strong reducing agents (sodium borohydride, borane complexes) unlike other nanoclusters and metal-ligand complex synthesis, here insulin acts a reducing agent and the synthesis process is speedy and completed within 4 hours whereas most of the syntheses reported earlier need a prolonged time for the reaction.

Instruments. MS of insulin-gold conjugates was measured using variable temperature - Nano electrospray ionization (VT-nanoESI) on a commercial quadrupole time-of-flight (micro-qTOF II, Bruker-Daltonics, Bremen, Germany). MALDI-TOF MS analysis was also conducted on ultrafleXtreme mass spectrometer (Bruker) in linear mode, equipped with 355 nm Nd:YAG laser. UV-vis absorption spectra were recorded with an AvaSpec2048FT spectrophotometer, the sample were illuminated with a continuous spectrum of halogen lamp coupled with an AvaLightDH-S deuterium lamp, and the transmitted light was collected and analyzed with the spectrophotometer. PL spectra were recorded using a Horiba Jobin Yvon Fluoromax4 spectrophotometer, and the data were collected with FluorEssence software. Circular dichroism was recorded by JASCO J815 CD spectropolarimeter. For CD measurements, we used both human and bovine insulin since their CD spectra are identical.[3] Fluorescence quantum yield was determined using integrating sphere in the FS5 Spectrofluorometer (Edinburgh Instruments). XPS measurements were carried out using a PHI Quantera SXM instrument (Physical Electronics, Chanhassen, USA) equipped with a 180° hemispherical electron energy analyzer and a monochromatized Al Kα (1486.6 eV) source operated at 15 kV and 4 mA. The analysis spot had a diameter of 200 µm and the detection angle relative to the substrate surface was 45°. Dynamic light scattering. Insulin samples were characterized in term of measurement of particle size distribution using dynamic light scattering. Measurements were performed on a Nanosizer system (Malvern Panalytical Ltd., Malvern, UK). Samples were first equilibrated at 20°C in the system, then three repeats of ten measurements were made in low-volume micro cuvette (BR759215- BRAND Life Science). The instrument settings were optimized automatically by means of the Zetasizer software (Malvern Panalytical Ltd., Malvern, UK).

Fluorescence lifetime was measured using time-correlated single-photon counting (TCSPC) method was applied to determine PL lifetime using the FS5 Spectrofluorometer (Edinburgh Instruments) equipped with a 405 nm diode laser as excitation source. Fluoracle software was used to determine the decay curve fitting with biexponential function:

$$I = A + B_1 e^{-\frac{t}{\tau_1}} + B_2 e^{-\frac{t}{\tau_2}}$$

The average lifetime was calculated by using the following equation.

$$< \tau_{int} > = \frac{B_1 \tau_1^2 + B_2 \tau_2^2}{B_1 \tau_1 + B_2 \tau_2}$$

where B_1, B_2 and average fluorescence lifetime (τ_{int}) are the contributions of particular lifetime. The χ^2 value determined the quality of fit. All spectroscopic measurements were done in a 1 cm quartz cuvette from Hellma GmbH at room temperature using air-saturated solutions.

Two-photon optical characterization. Two-photon excited luminescence was measured using a custom-built multiphoton microscope consisting of a femtosecond mode-locked Ti:sapphire laser (~100 fs, 80 MHz, Chameleon,

Coherent Inc.) with an incident wavelength range tunable within λ = 700–1050 nm. Luminescence was recorded through a microscope objective (Nikon Plan Fluor, 40×, NA 0.75), and 2PEL signals were recorded in the epifluorescence mode. 2PEL spectra were measured with a Shamrock 303i spectrometer (Andor) equipped with an iDus camera (Andor). Samples and references were illuminated with the output power of 70 mW Luminescence was collected in parallel shortpass filter (cut-off wavelength 750 nm). In order to exclude the potential excitation at lower wavelength range 700 nm long-pass filters were applied. Measurement conditions were set the same for each sample and reference sample. The experimental conditions were chosen to prevent photobleaching and achieve a high signal to noise ratio. Two-photon absorption cross sections were calculated with the equation:

$$\sigma_{2,S} = \frac{F_{2,S(\lambda_{exc})} C_r \varphi_r n_r^2}{F_{2,r}(\lambda_{exc}) C_s \varphi_s n_s^2} \sigma_{2,r}$$

Two-photon brightness was calculated with equation:

$$\sigma_{2,S,eff} = \sigma_{2,S} * \varphi_s$$

where C is the fluorophore molar concentration, n the refractive index of the solvent, φ the photoluminescence quantum yield, and F is integrated two-photon photoluminescence intensity at particular excitation wavelength. The letters s and r correspond to the sample and reference, respectively. The chosen reference was a Rhodamine B solution in MeOH. The two-photon absorption cross section of Rhodamine B was obtained from elsewhere.[4]

Mass spectrometry characterization. MALDI-TOF MS analysis was conducted on ultrafleXtreme mass spectrometer (Bruker) in linear mode, equipped with 355 nm Nd:YAG laser, with 2,5-dihydroxybenzoic acid (DHB) as the matrix substance.[5] Both Insulin and Insulin-Au were prepared on a steel target by the "dried droplet" method as following description: The saturated DHB matrices solutions (10 mg/mL) were prepared in water-acetonitrile (50/50 vol. with 0.1% trifluoroacetic acid). 5 μL Au-Insulin solution (in 50/50 water-acetonitrile) was mixed with 10 μL saturated matrix under agitation (equivalent ratio 2:1). 1 μL of mixture was deposited to the groundsteel target with drying at ambient temperature. Electro-Spray MS were recorded on commercial quadrupole time-of-flight (micro-qTOF II, Bruker-Daltonics, Bremen, Germany, mass resolution 10,000) instrument. The thermalized nano-ESI source (homemade) maintained a temperature at 17°C. The solution was desalted by acetic acid addition, ultrafiltration and acetic ammonium addition.

Polyacrylamide gel electrophoresis (PAGE). PAGE separation was carried out using a vertical gel electrophoresis unit with a size of 0.2cm*10cm*10cm. The separating and stacking gels were prepared by acrylamide monomers with the total contents of 12 and 5 wt% (acrylamide–bis-(acrylamide) 96 : 4), respectively. The running buffer consisted of 250 mM glycine, 25 mM tris(hydroxymethylamine), and 0.1% sodium dodecyl-sulfate (SDS). The as-prepared Au-Insulin were dissolved in a 25% (v/v) glycerol–water solution. The sample solutions were loaded onto the stacking gel (50 μL per well) and eluted for 3 h at a constant voltage mode (150 V) to achieve sufficient separation.

Reactive oxygen species generation measurement. The singlet oxygen generation efficiency was measured by an indirect method with the $^1O_2$ sensor of 1,3-diphenylisobenzofuran (DPBF). Singlet oxygen generation was monitored under the excitation at 473 nm using a continuous wavelength laser (Changchun New Industries Optoelectronics Tech. Co., Ltd, China) with an output power of 250 mW and a beam diameter of 3 mm. A typical solution used in the experiment contained photosensitizers and DPBF with a concentration of 1.37 × 10^{-6} M and 6.15 × 10^{-5} M, respectively. All solutions were prepared in ethanol. The samples were loaded in quartz cuvettes (1cm light path length) and the absorbance was recorded with irradiation for different time. The singlet oxygen quantum yield was calculated from the chemical quenching of DPBF, with a comparative method with new Methylene Blue (NMB) as reference. By a comparative method as known $^1O_2$ quantum yield for new methylene blue (NMB) was $\phi_{\Delta}^{NMB} = 0.65$.[6] The $^1O_2$ quantum yield for insulin-Au conjugates could be calculated by eqn:

$$\phi_{\Delta}^{AuIns} = \frac{Slope^{\mathrm{AuIns}}}{Slope^{\mathrm{NMB}}} \times \frac{1 - 10^{-Abs_{473}^{\mathrm{NMB}}}}{1 - 10^{-Abs_{473}^{\mathrm{AuIns}}}} \times \phi_{\Delta}^{\mathrm{NMB}}$$

From absorption spectra, $Abs_{473}^{\mathrm{AuIns}} = 0.00459$, $Abs_{473}^{\mathrm{NMB}} = 0{,}00101$. With the slope value by linear fitting in Figure S5, the $^1O_2$ quantum yield for insulin-gold under laser excitation at 473 nm was calculated as $\phi_{\Delta}^{AuIns} = 0.0970$, respectively.

Data Analysis. The consistency of given measurement of two-photon excited luminescence (TPEL) spectra is assured by at least three cycles of repetition of the exact same spectra of particular sample at specific wavelength. Averaged TPEL spectra are further used for calculations of two-photon brightness. Besides, two photon brightness is calculated from several variables, e.g. integrated fluorescence intensity of analyzed sample and reference sample, quantum yield (QY) of our sample, QY and two-photon absorption cross-section (σ_2) found in the literature for specific reference dye. Therefore,

error bars calculated for each two-photon brightness value in Figure 2 already consist of errors from: our measurements of TPEL and QY of insulin-Au sample as well as the literature data on QY and σ_2 of reference sample. Standard deviation of repeatability of the experiment should not exceed the one calculated as partial derivatives from errors of those several variables. Final uncertainty of two-photon brightness value is found to be below 15%. The singlet oxygen generation efficiency and quantum yield were measured repeatly for 3 times and the standard deviations plotted as the error bar. Besides, the standard deviations from absorption value , linear fitting and calculation were taken into account, and we got the $^1O_2$ generation rate of insulin-Au conjugates as 1.5±0.3, the $^1O_2$ generation quantum yield quantum yield as 13%±5%.

Computational. The structural optimization of the systems presented in this work was carried out using density functional theory, and its B3LYP functional[7-8] in combination with triple zeta plus polarization atomic basis set (def2-TZVP)[9]. The 19 electron relativistic effective core potential developed by the Stuttgart group[10] was used to describe Au atoms.

The optical properties of the neutral and charged forms of Tyrosine were obtained using B3LYP functional[7-8] and def2-TZVP basis set[9]. For the Tyrosine-gold complexes we employed the long-range corrected version of the hybrid B3LYP functional using the Coulomb attenuated method (CAM-B3LYP),[11] due to the charge-transfer character of the transitions. The largest system modeled consists of three tyrosines and one gold atom (3Tyr+Au(III)). NH_2 and COOH groups in the backbone of tyrosine in the 3Tyr+Au(III) system were replaced by CH_3 groups to model presence of other aminoacids in insulin which surround three tyrosines.

Structural and linear optical properties were calculated using Gaussian program[12] while nonlinear optical properties of the 3Tyr+Au(III) systems were calculated using the DALTON[13] quantum chemistry program.[14] Implicit water effects were incorporated using the Polarizable Continuum Model with integral equation formalism variant.

Gromacs version 2020.4[31] was used for all-atom MD simulation of insulin in explicit solvent. Force field amber99sb[32] with the SPCE water model[33] was used. The simulation was done at 300 K and 1 bar, using the isothermal−isobaric (NPT) ensemble. Insulin was placed into a dodecahedral box of water with at least of 12 nm between the edges of a box and protein atoms. Periodic boundary conditions were employed. Counterions (Na+ and Cl-) replaced solvent molecules to neutralize the protein net charge. We used three step equilibration: (i) the steepest descent (10000 steps) energy minimization; (ii) solvent equilibration with restrained atomic positions of the insulin using a harmonical potential (100 ps at 298 K); (iii) system equilibration to set the temperature at 298 K and pressure at 1 bar (100 ps each). We used a time-step of a 2 fs. The LINCS algorithm[34] was used to constrain heavy atom bonds, long-range electrostatic interactions were calculated using the Particle Mesh Ewald (PME) summation scheme[35] and van der Waals and short-range Coulomb interactions were cut at 0.9 nm.

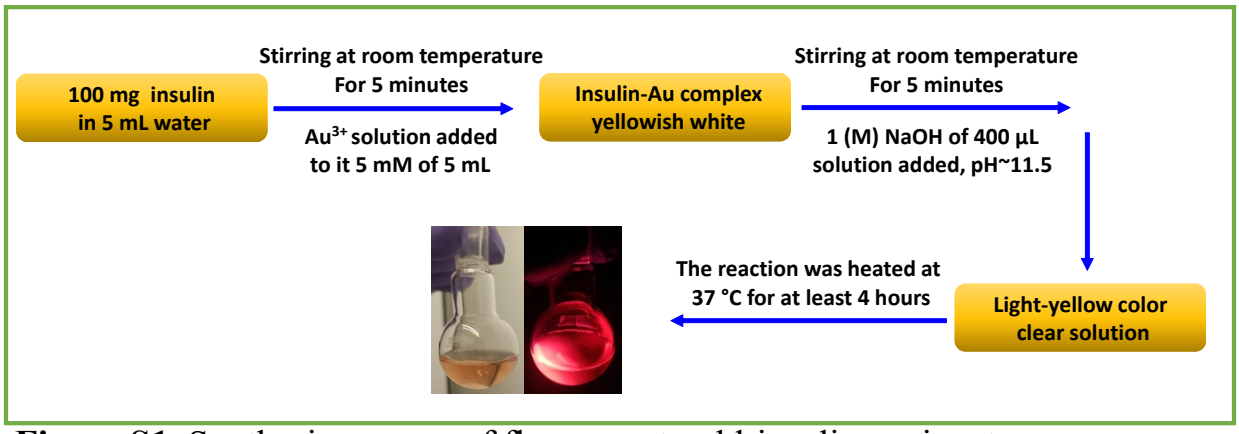

Figure S1. Synthesis process of fluorescent gold-insulin conjugates.

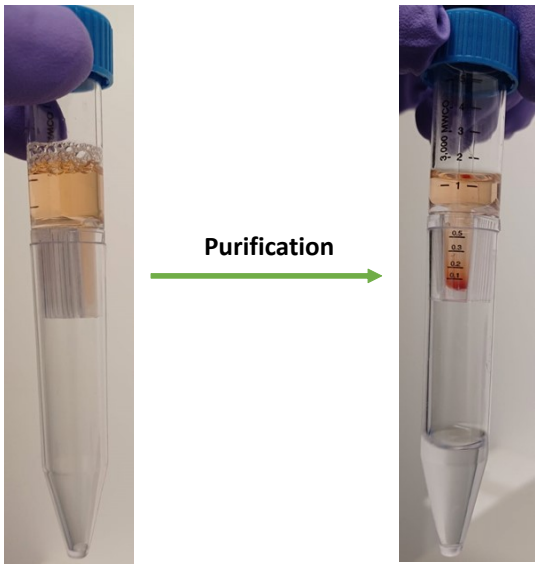

Figure S2. Purification of insulin-gold conjugates by using centrifugation with 3kDa MWCO.

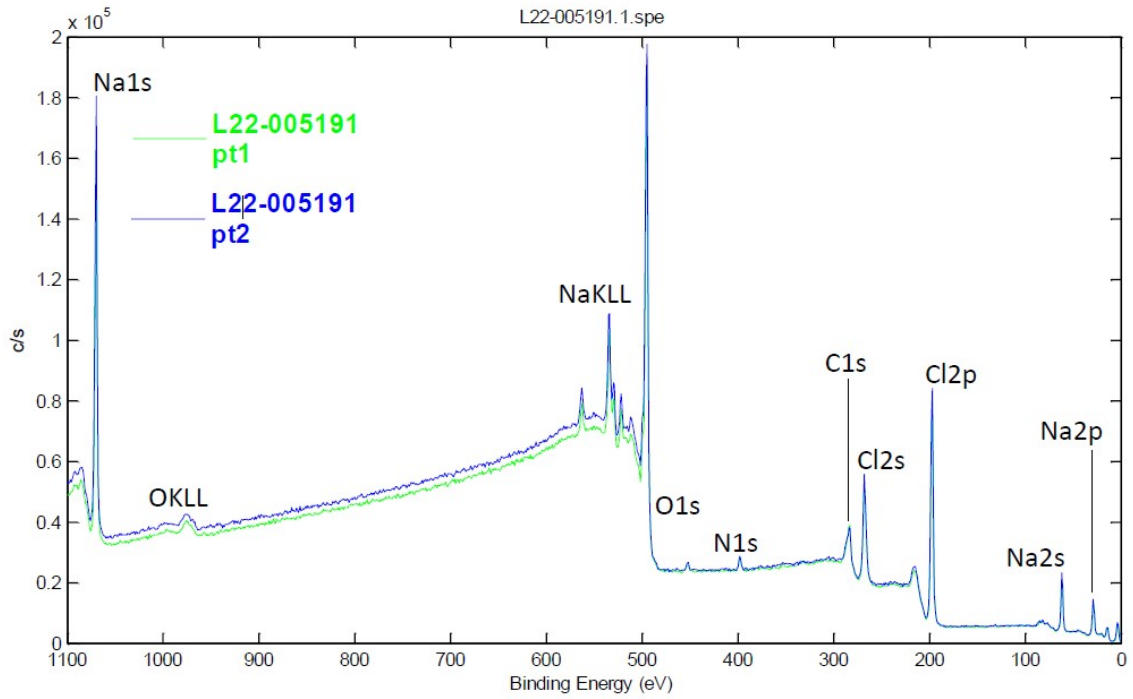

Figure S3 : Elemental XPS analysis of gold-insulin conjugates (2 samples in powder film).

	sample	C	O	N	Au
Au-INSU (% content)	pt1	69,2	21,1	9,4	0,3
	pt2	67,2	24,7	7,8	0,3
Theoretical ($C_{257}N_{65}O_{77}Au$)		64,1	19,3	16,3	0,3

Table S1 : Quantitative XPS results of Au-insulin sample spectrum of which has been recorded in four subsequent measurements in order to determine the effect of X-ray irradiation on the chemical state of the sample.

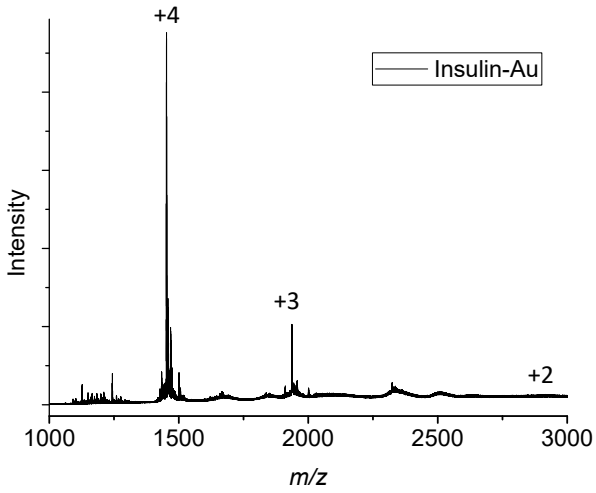

Figure S4: Full ESI-MS spectrum of gold-insulin conjugates. Assigned charge states have been labeled.

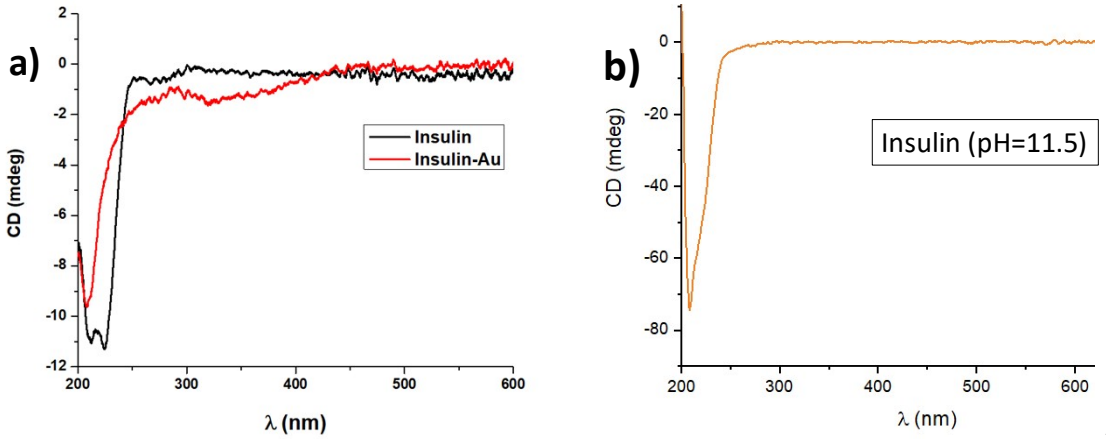

Figure S5. a) Circular dichroism spectra of insulin (a) and insulin-Au conjugates (b). Circular dichroism spectrum of insulin is recorded at neutral pH (i.e., insulin in water). **b)** Circular dichroism spectra of insulin at pH=11.5.

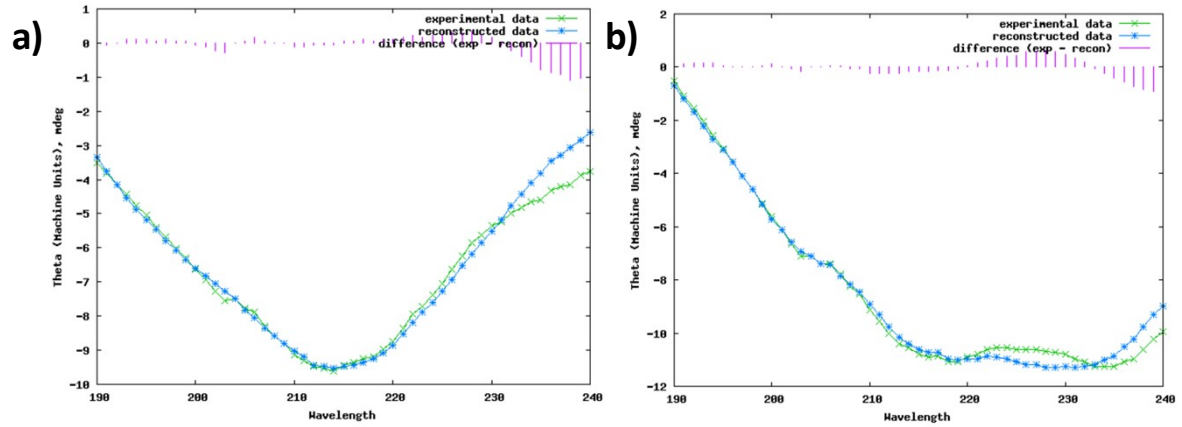

Figure S6. Experimental and simulated circular dichroism spectra of insulin-gold conjugate (a) and insulin at neutral pH (b) and.

Table S2. Secondary structure of insulin and insulin-Au.

	Helix 1	Helix 2	Strand 1	Strand 2	Turns	Unordered	Total
Insulin	0.04	0.13	0.18	0.11	0.28	0.27	1.01
Insulin-gold	0.02	0.08	0.20	0.12	0.25	0.33	1

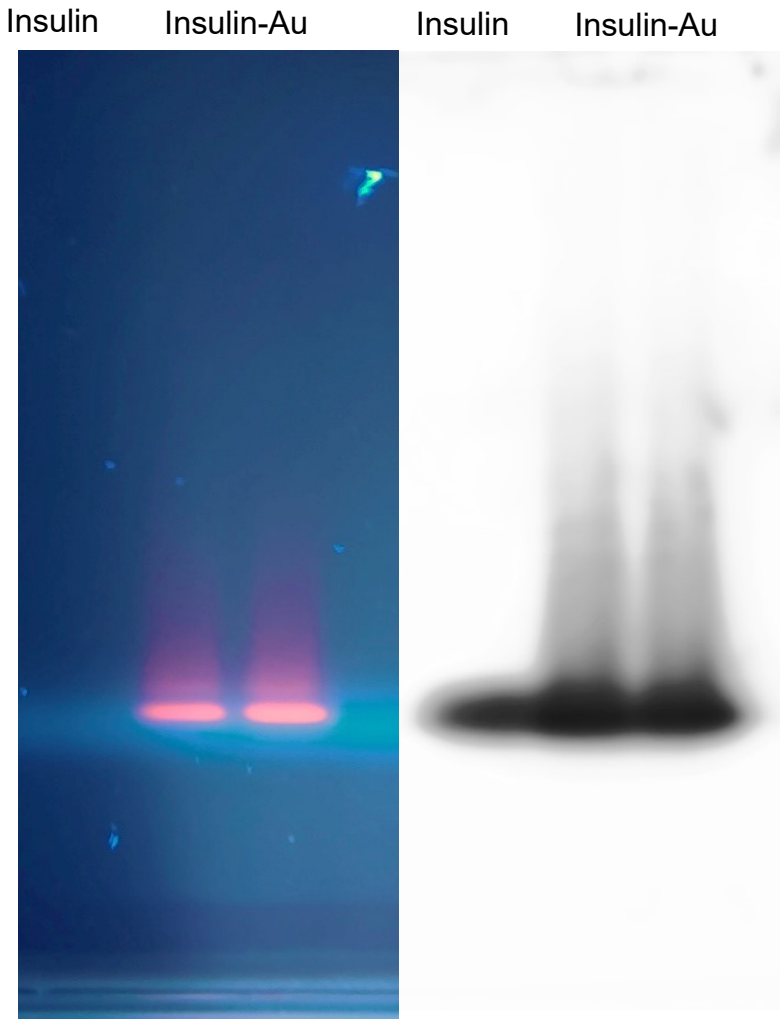

Figure S7. Photo of gel band of Insulin and Insulin-Au (two measurements) after polyacrylamide gel electrophoresis, under 365 nm UV light (left) and under daylight with protein staining (right).

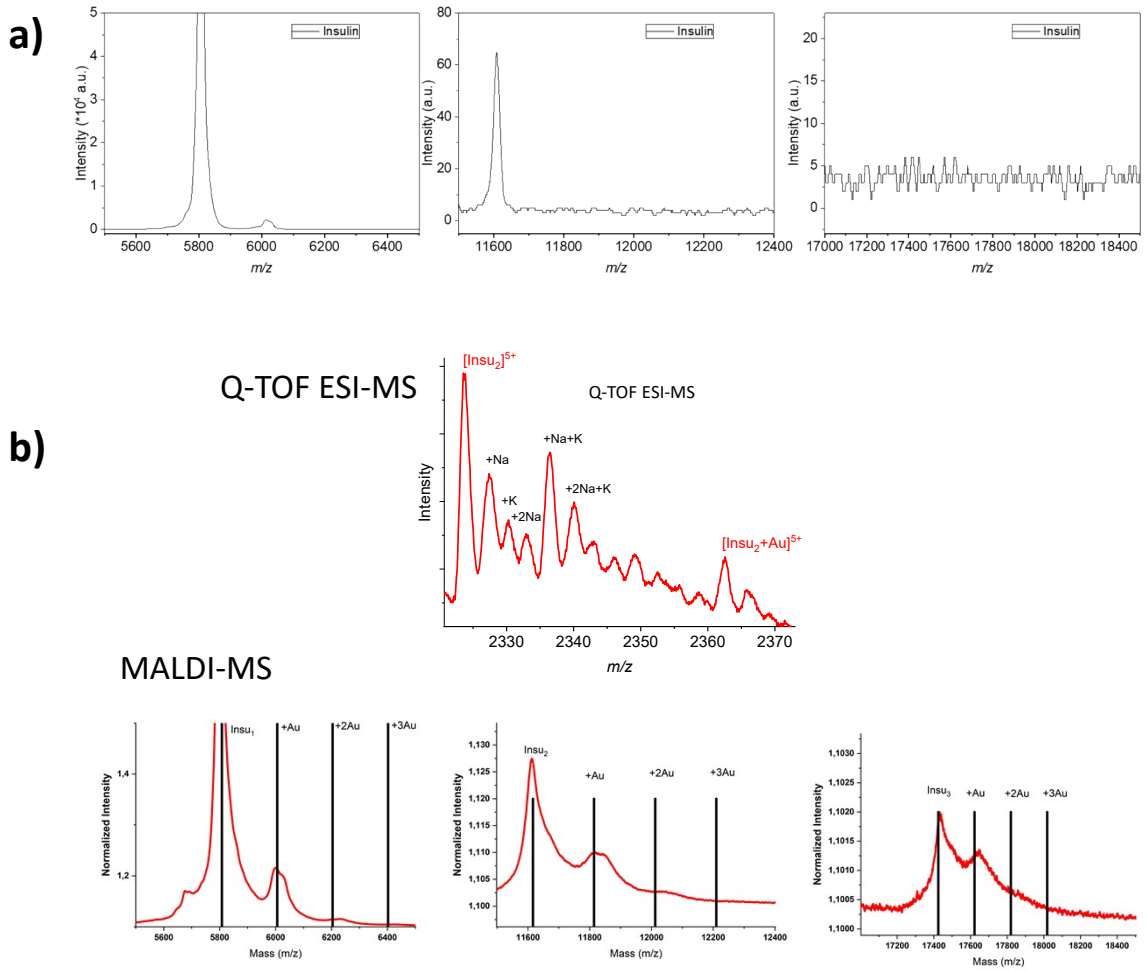

Figure S8. MS spectra of oligomers of a) insulin and b) insulin-gold conjugates.

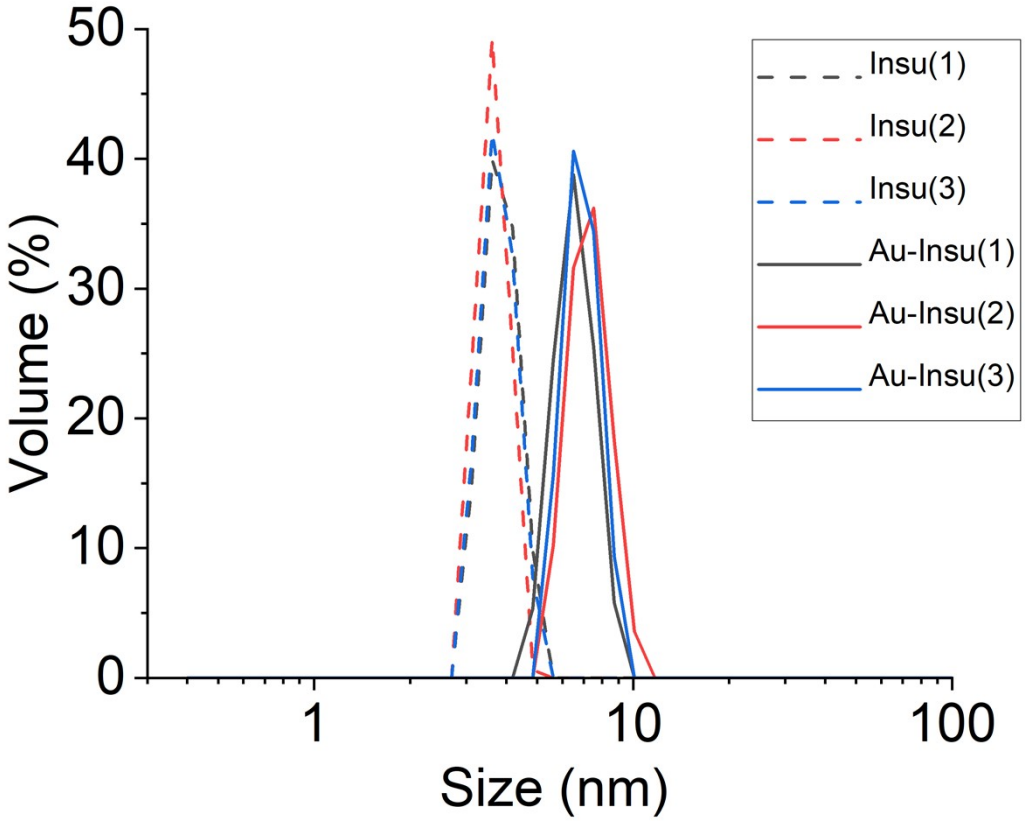

Figure S9. Dynamic light scattering (DLS) of insulin and insulin-Au conjugates. Measurements done with 3 replicates.

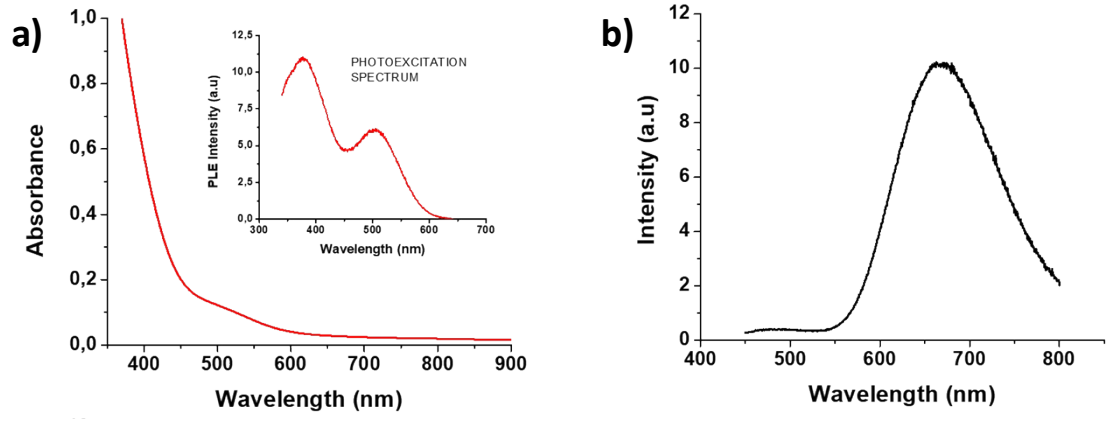

Figure S10. Absorption spectrum (a) and photoluminescence emission spectrum (b) of insulin-gold conjugate. Inset: photoluminescence excitation spectrum of insulin-gold.

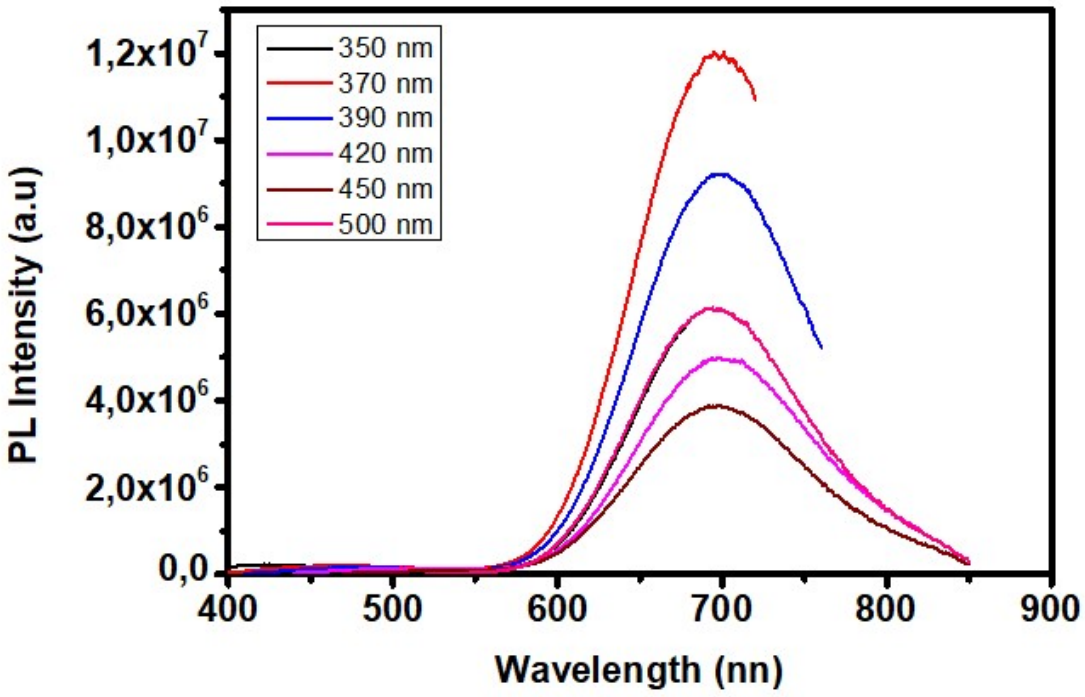

Figure S11. Emission spectra of insulin-Au conjugates at different excitation wavelengths.

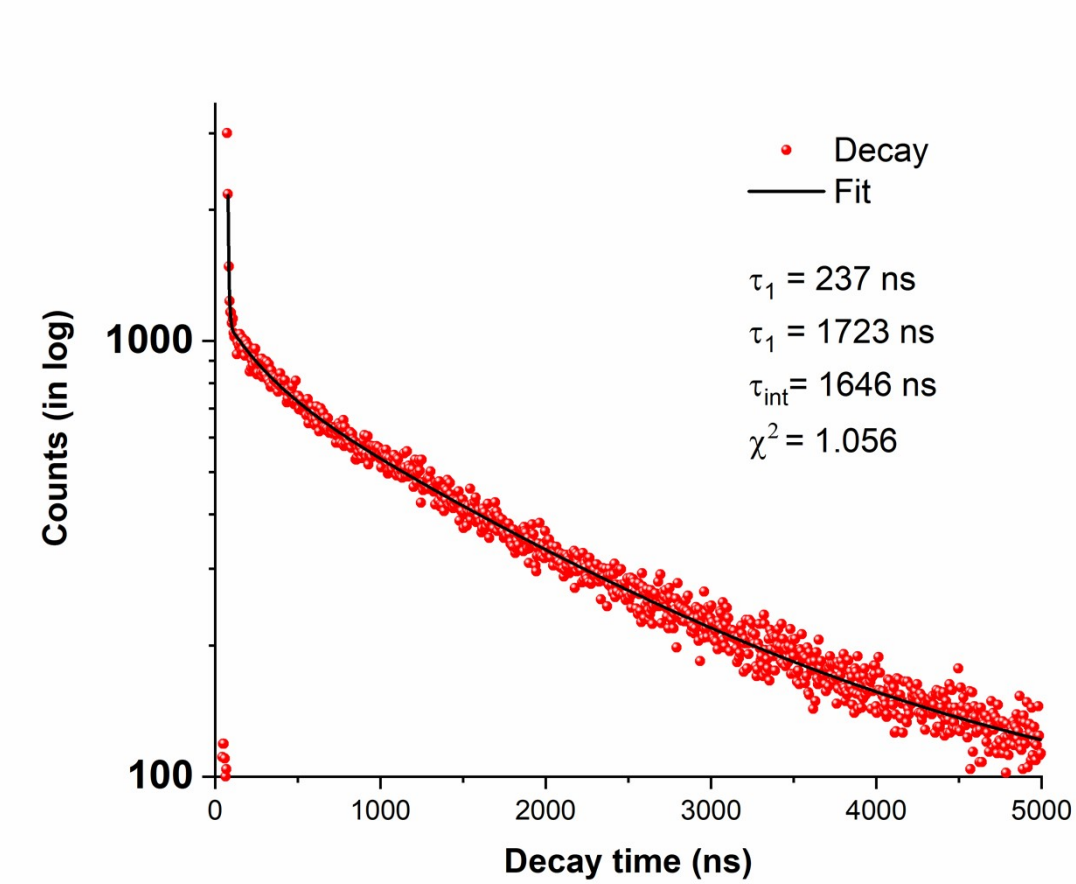

Figure S12. Photoluminescence lifetime decay curve of Insulin-Au conjugate.

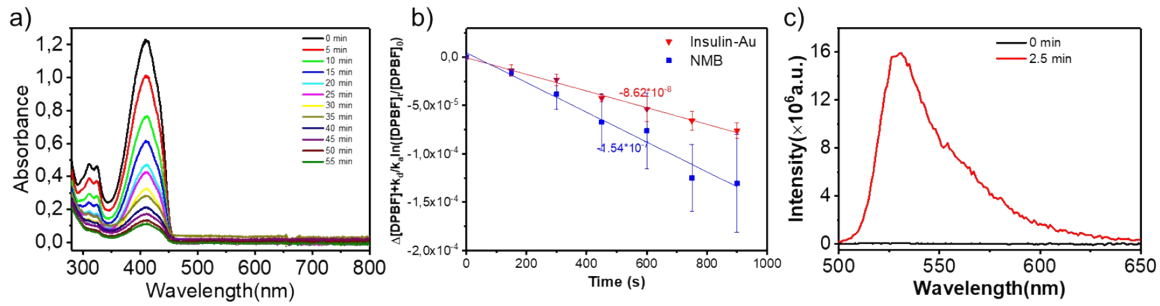

Figure S13. (a) Absorption spectra evolution of DPBF-insulin-gold mixture solution under cw 473 nm laser irradiation. (b) Comparison of the changes in $\Delta[DPBF]+k_d/k_a \ln([DPBF]_t/[DPBF]_0)$ with time for insulin-gold (red) and NMB (blue) under laser excitation at 473 nm. (c) Fluorescence spectra of DCF and insulin-gold mixture solution with 473 nm cw laser irradiation for 0 min and after 2.5 min. Fluorescence of DCF was recorded with excitation wavelength at 488 nm.

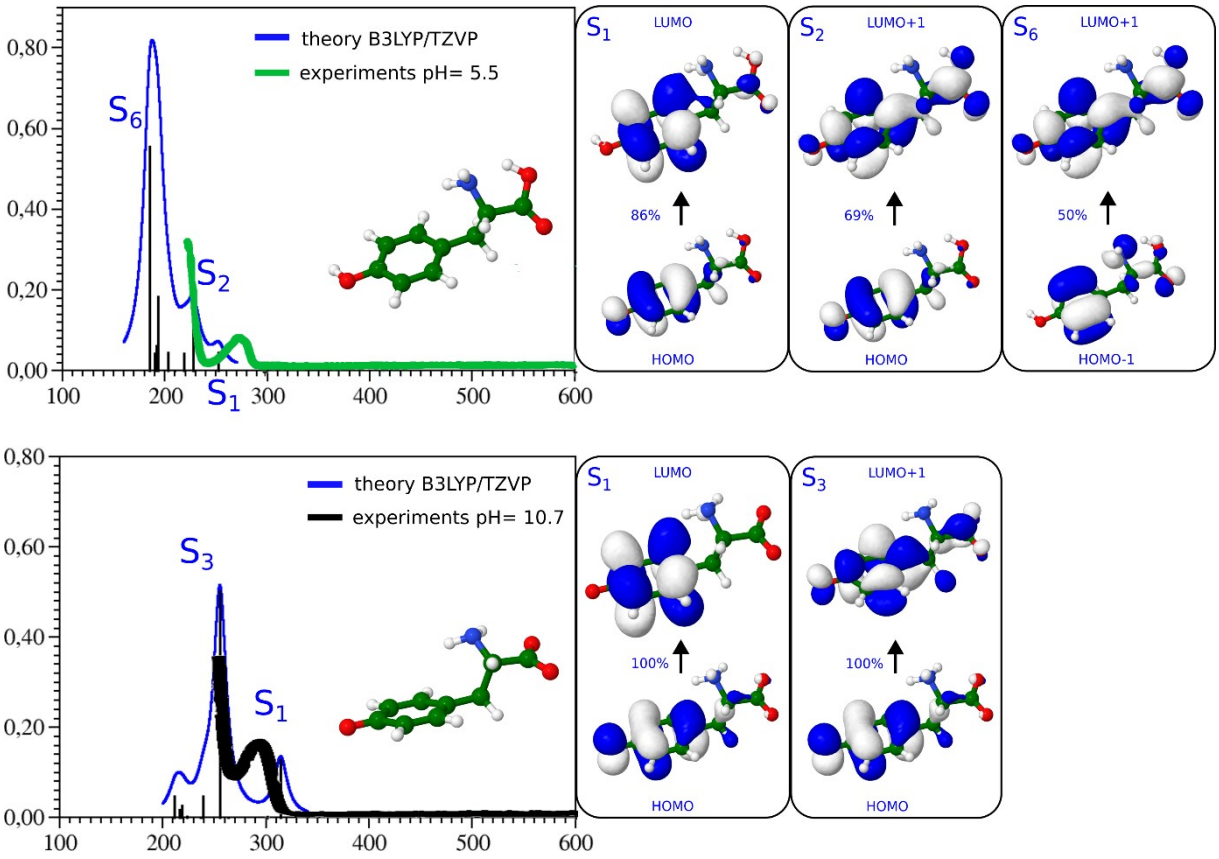

Figure S14. Experimental and TD-DFT absorption spectra and lowest energy structures of tyrosine at different pH. Leading excitations responsible for the characteristic features of absorption are illustrated on the right side. At pH=5.5, both carboxylic and phenolic groups are neutral. At pH=10.7, both carboxylic and phenolic groups re in deprotonated forms. Experimental spectra are recorded in water and implicit water was used for calculations.

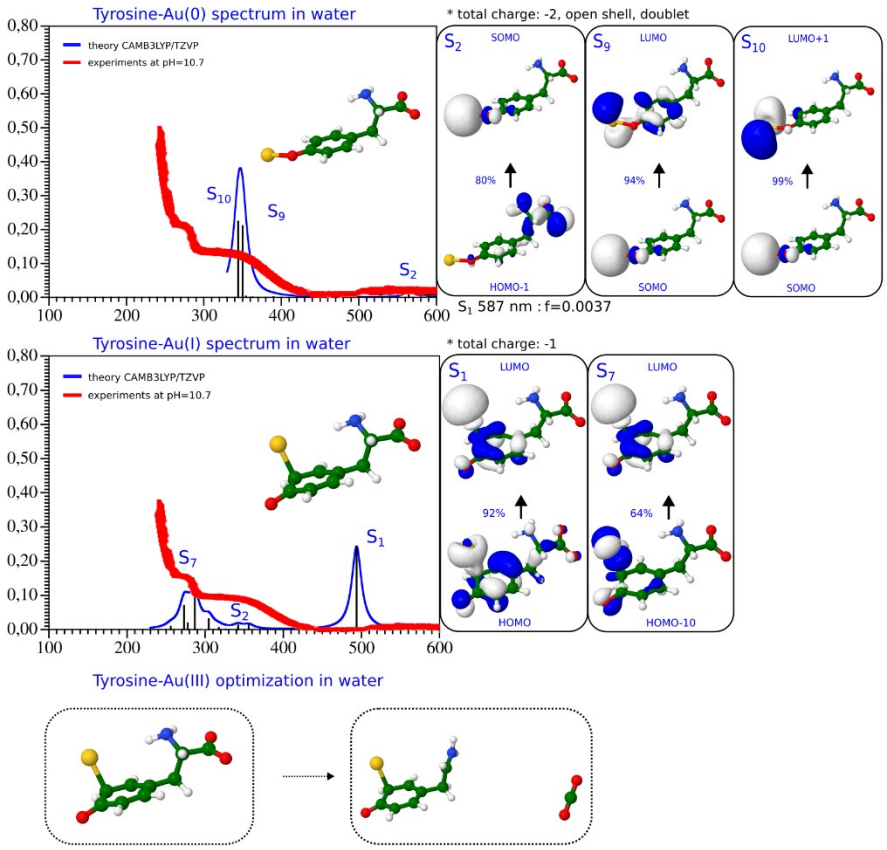

Figure S15. Experimental and TD-DFT absorption spectra and lowest energy structures of doubly deprotonated tyrosine complexed with Au(0) (top panel) and Au(I) (bottom panel). Leading excitations responsible for the characteristic features of absorption are illustrated on the right side. Experimental spectra are recorded in water and implicit water was used for calculations. When trying to optimize the structure of tyrosine with Au(III), fragmentation of tyrosine occurred, which indicated the instability of this structure (bottom panel).

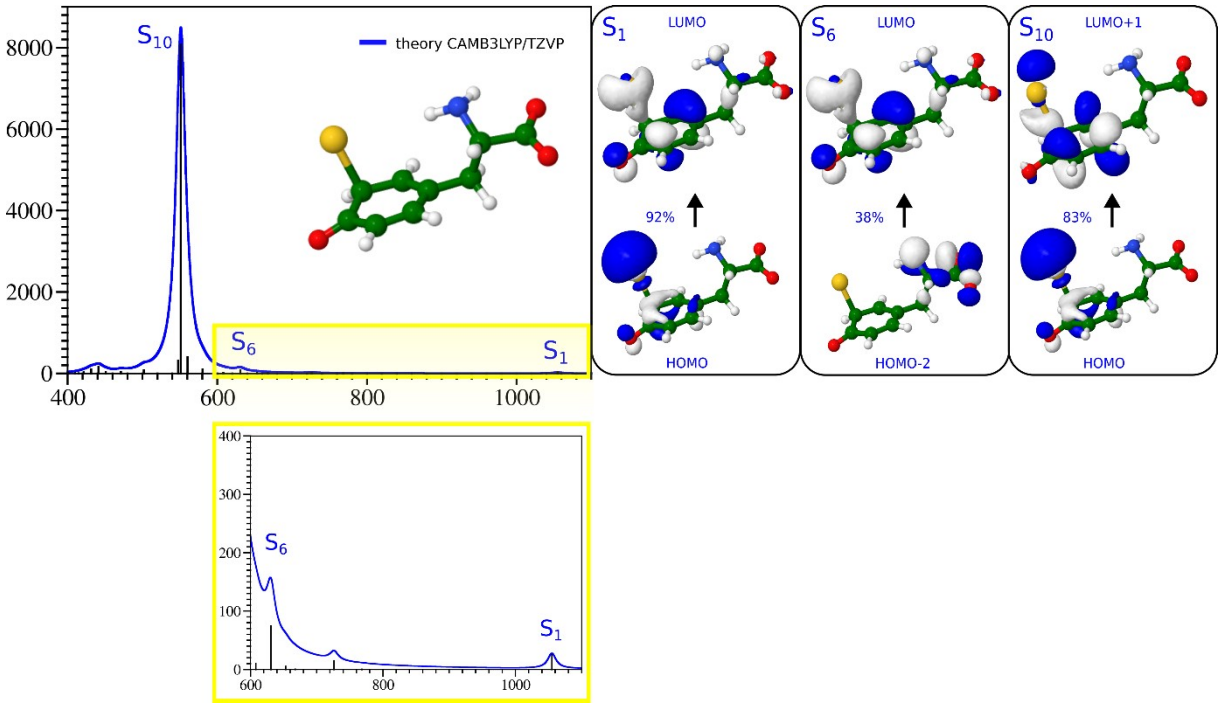

Figure S16. TD-DFT results on two-photon (TPA) absorption of Tyrosine complexed with Au(I) and responsible excitations. X axes are wavelengths in nm, and y axes are cross sections in GM units.

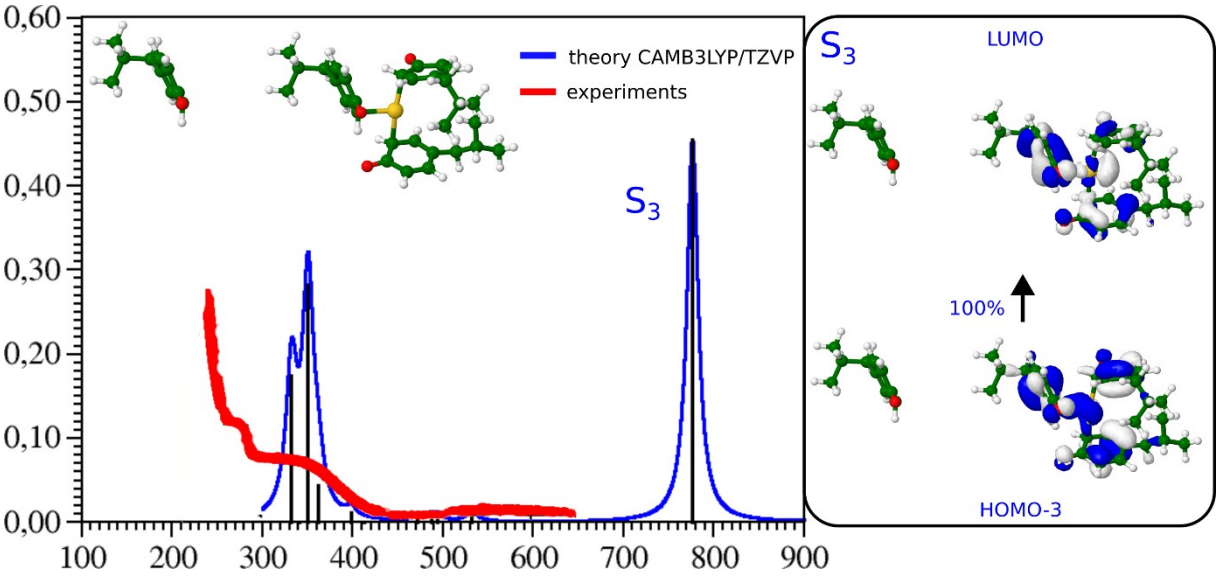

Figure S17: Absorption spectrum of Tyr4+Au(III), where Au(III) is coordinated to 3 tyrosines, and the fourth Tyr is placed away from them.

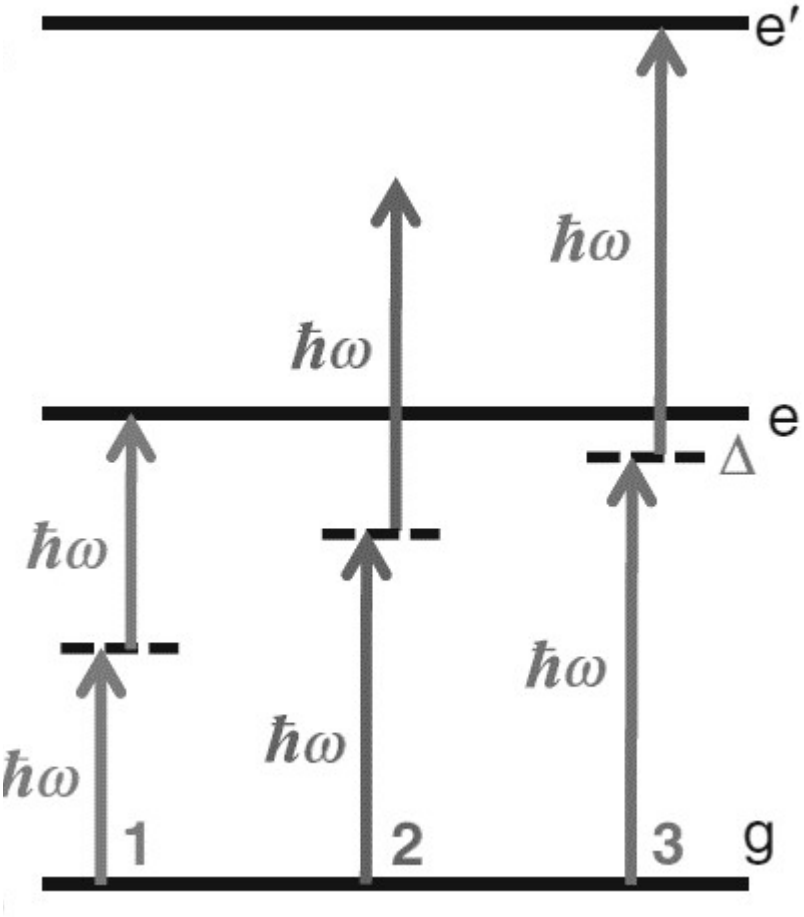

Scheme S1: Schematic of frequency degenerate two-photon absorption (TPA) : (1) into the first allowed singlet state, (2) above the first allowed singlet state, and (3) a double resonant condition, with a small intermediate state resonance energy difference, Δ, and a transition into an allowed final TPA state.

References

1. Liu, C.-L.; Wu, H.-T.; Hsiao, Y.-H.; Lai, C.-W.; Shih, C.-W.; Peng, Y.-K.; Tang, K.-C.; Chang, H.-W.; Chien, Y.-C.; Hsiao, J.-K.; Cheng, J.-T.; Chou, P.-T., Insulin-Directed Synthesis of Fluorescent Gold Nanoclusters: Preservation of Insulin Bioactivity and Versatility in Cell Imaging. *Angewandte Chemie International Edition* **2011,** *50* (31), 7056-7060.
2. Mittal, R.; Gupta, N., pH-dependent Synthesis and Interactions of Fluorescent L-Histidine Capped Copper Nanoclusters with Metal Ions. *Journal of Fluorescence* **2023**, https://doi.org/10.1007/s10895-023-03433-7.
3. Mishra, N. K.; Joshi, K. B.; Verma, S., Inhibition of Human and Bovine Insulin Fibril Formation by Designed Peptide Conjugates. *Molecular Pharmaceutics* **2013,** *10* (10), 3903-3912.
4. Makarov, N. S.; Drobizhev, M.; Rebane, A., Two-photon absorption standards in the 550–1600 nm excitation wavelength range. *Opt. Express* **2008,** *16* (6), 4029-4047.
5. Yuan, H.; Lima, D.; Comby-Zerbino, C.; Bouanchaud, C.; Chirot, F.; Bain, D.; Zhang, S.; Antoine, R., Assessing the matrix effects on MALDI-MS in the positive and negative ion mode detection for protein-protected metal nanoclusters. *Int. J. Mass Spectrom. (under review)* **2024**, ChemRxiv. 2024; doi:10.26434/chemrxiv-2024-l8vjm.
6. Ronzani, F.; Trivella, A.; Arzoumanian, E.; Blanc, S.; Sarakha, M.; Richard, C.; Oliveros, E.; Lacombe, S., Comparison of the photophysical properties of three phenothiazine derivatives: transient detection and singlet oxygen production. *Photochemical & Photobiological Sciences* **2013,** *12* (12), 2160-2169.
7. Becke, A. D., A New Mixing of Hartree-Fock and Local Density-Functional Theories. *J. Chem. Phys.* **1993,** *98* (2), 1372-1377.
8. Lee, C. T.; Yang, W. T.; Parr, R. G., Development of the Colle-Salvetti correlation-energy formula into a functional of the electron density. *Phys Rev. B* **1988,** *37*, 789.
9. Weigend, F.; Ahlrichs, R., Balanced basis sets of split valence, triple zeta valence and quadruple zeta valence quality for H to Rn: Design and assessment of accuracy. *Phys. Chem. Chem. Phys.* **2005,** *7*, 3297.
10. Andrae, D.; Haeussermann, U.; Dolg, M.; Stoll, H.; Preuss, H., Energy-adjusted ab initio pseudopotentials for the second and third row transition elements. *Theor. Chim. Acta* **1990,** *77*, 123.
11. Yanai, T.; Tew, D. P.; Handy, N. C., *Chem. Phys. Lett.* **2004,** *393*, 51-57.
12. Frisch, M. J.; Trucks, G. W.; Schlegel, H. B.; Scuseria, G. E.; Robb, M. A.; Cheeseman, J. R.; Scalmani, G.; Barone, V.; Petersson, G. A.; Nakatsuji, H.; Li, X.; Caricato, M.; Marenich, A. V.; Bloino, J.; Janesko, B. G.; Gomperts, R.; Mennucci, B.; Hratchian, H. P.; Ortiz, J. V.; Izmaylov, A. F.; Sonnenberg, J. L.; Williams; Ding, F.; Lipparini, F.; Egidi, F.; Goings, J.; Peng, B.; Petrone, A.; Henderson, T.; Ranasinghe, D.; Zakrzewski, V. G.; Gao, J.; Rega, N.; Zheng, G.; Liang, W.; Hada, M.; Ehara, M.; Toyota, K.; Fukuda, R.; Hasegawa, J.; Ishida, M.; Nakajima, T.; Honda, Y.; Kitao, O.; Nakai, H.; Vreven, T.; Throssell, K.; Montgomery Jr., J. A.; Peralta, J. E.; Ogliaro, F.; Bearpark, M. J.; Heyd, J. J.; Brothers, E. N.; Kudin, K. N.; Staroverov, V. N.; Keith, T. A.; Kobayashi, R.; Normand, J.; Raghavachari, K.; Rendell, A. P.; Burant, J. C.; Iyengar, S. S.; Tomasi, J.; Cossi, M.; Millam, J. M.; Klene, M.; Adamo, C.; Cammi, R.; Ochterski, J. W.; Martin, R. L.; Morokuma, K.; Farkas, O.; Foresman, J. B.; Fox, D. J. *Gaussian 16 Rev. C.01*, Wallingford, CT, 2016.

13. Aidas, K.; Angeli, C.; Bak, K. L.; Bakken, V.; Bast, R.; Boman, L.; Christiansen, O.; Cimiraglia, R.; Coriani, S.; Dahle, P.; Dalskov, E. K.; Ekström, U.; Enevoldsen, T.; Eriksen, J. J.; Ettenhuber, P.; Fernández, B.; Ferrighi, L.; Fliegl, H.; Frediani, L.; Hald, K.; Halkier, A.; Hättig, C.; Heiberg, H.; Helgaker, T.; Hennum, A. C.; Hettema, H.; Hjertenæs, E.; Høst, S.; Høyvik, I.-M.; Iozzi, M. F.; Jansík, B.; Jensen, H. J. A.; Jonsson, D.; Jørgensen, P.; Kauczor, J.; Kirpekar, S.; Kjærgaard, T.; Klopper, W.; Knecht, S.; Kobayashi, R.; Koch, H.; Kongsted, J.; Krapp, A.; Kristensen, K.; Ligabue, A.; Lutnæs, O. B.; Melo, J. I.; Mikkelsen, K. V.; Myhre, R. H.; Neiss, C.; Nielsen, C. B.; Norman, P.; Olsen, J.; Olsen, J. M. H.; Osted, A.; Packer, M. J.; Pawlowski, F.; Pedersen, T. B.; Provasi, P. F.; Reine, S.; Rinkevicius, Z.; Ruden, T. A.; Ruud, K.; Rybkin, V. V.; Sałek, P.; Samson, C. C. M.; de Merás, A. S.; Saue, T.; Sauer, S. P. A.; Schimmelpfennig, B.; Sneskov, K.; Steindal, A. H.; Sylvester-Hvid, K. O.; Taylor, P. R.; Teale, A. M.; Tellgren, E. I.; Tew, D. P.; Thorvaldsen, A. J.; Thøgersen, L.; Vahtras, O.; Watson, M. A.; Wilson, D. J. D.; Ziolkowski, M.; Ågren, H., The Dalton quantum chemistry program system. *Wiley Interdisciplinary Reviews: Computational Molecular Science* **2014,** *4* (3), 269-284.
14. Fakhouri, H.; Bakulić, M. P.; Zhang, I.; Yuan, H.; Bain, D.; Rondepierre, F.; Brevet, P.-F.; Maršić, Ž. S.; Antoine, R.; Bonačić-Koutecký, V.; Maysinger, D., Ligand impact on reactive oxygen species generation of Au10 and Au25 nanoclusters upon one- and two-photon excitation. *Communications Chemistry* **2023,** *6* (1), 97.